Inorganic Chemistry

Article

An Application of the "Coloring Problem":
Structure–Composition–Bonding Relationships in the Magnetocaloric
Materials LaFe$_{13-x}$Si$_x$

Mi-Kyung Han and Gordon J. Miller*

Department of Chemistry, Iowa State University, Ames, Iowa 50011

The LaFe$_{13-x}$Si$_x$ ($1.0 \leq x \leq 5.0$) series is studied experimentally and theoretically to gain possible understanding for the relationships among geometrical structure, chemical composition, magnetic behavior, and physical properties as related to the magnetocaloric effect in these compounds. As the Si concentration increases, LaFe$_{13-x}$Si$_x$ exhibits a structural transformation from the cubic NaZn$_{13}$ structure type to a tetragonal derivative due primarily to preferential ordering of Fe and Si atoms. At room temperature, LaFe$_{13-x}$Si$_x$ crystallize in the cubic structure for the range $1 \leq x \leq 2.6$ and in the tetragonal for $3.2 \leq x \leq 5$. In the range $2.6 \leq x \leq 3.2$, it shows a two-phase mixture. Temperature-dependent *single-crystal* X-ray diffraction experiments near the corresponding Curie temperatures were performed on the room-temperature cubic phases to examine the origin of the large isothermal magnetic entropy changes. A thorough statistical and structural analysis of the data indicates that the noncentrosymmetric $F\bar{4}3c$ space group provides a more adequate atomic arrangement than the centrosymmetric $Fm\bar{3}c$ space group. This change in space group leads to divergence for specific sets of Fe–Fe distances below the Curie temperature that arises from tilting of Fe-centered [Fe$_{12-x}$Si$_x$] icosahedra. The noncentrosymmetric space group also agrees with the predominance of icosahedral clusters lacking local inversion symmetry. From extended Hückel and tight-binding linear muffin-tin orbital (TB-LMTO) electronic structure calculations on various model structures, the $F\bar{4}3c$ model is more energetically favorable than the $Fm\bar{3}c$ model. Extended Hückel calculations on various icosahedral [Fe$_{12-n}$Si$_n$] ($n = 1–5$) clusters and TB-LMTO calculations on "LaFe$_{13}$," LaFe$_{11}$Si$_2$, and LaFe$_9$Si$_4$ have also been carried out to study the effects of a main group element (Si) on stabilizing the cubic NaZn$_{13}$-type structure, influencing the transformation between cubic and tetragonal symmetries, and to study relationships among their chemical bonding and magnetic properties.

Introduction

Environmentally friendly, alternative refrigeration technology near ambient conditions is a subject of current interest as a means to replace conventional, ozone-depleting refrigeration materials. One possibility, magnetic refrigeration, offers an energy efficient and ecologically clean cooling method over a wide temperature range[1−4] and has been a research focus over the past decade since the discovery of a giant magnetocaloric effect (MCE) in Gd$_5$Si$_2$Ge$_2$ at 276 K.[5] In this and related RE_5(Si$_x$Ge$_{1-x}$)$_4$ examples, a giant MCE occurred when the ferromagnetic−paramagnetic transition accompanied a change in crystal structure.[3,5,6] Subsequently, many other materials have been studied with respect to their magnetocaloric properties and possible applications.[3]

Systems containing 3d metals like Mn, Fe, or Co may also show magnetic transitions near ambient temperatures with large changes in magnetization, like, for example, the series LaFe$_{13-x}$Si$_x$.[7] As the Si composition in LaFe$_{13-x}$Si$_x$ increases from $x = 1.5$ to 2.5, the Curie temperature (T_C) also increases

---

* To whom corespondence should be addressed. E-mail: gmiller@iastate.edu.

(1) Brown, G. V. *J. Appl. Phys.* **1976**, *47*, 3673.
(2) Pecharsky, V. K.; Gschneidner, K. A., Jr. *J. Magn. Magn. Mat.* **1999**, *200*, 44.
(3) Gschneidner, K. A., Jr.; Pecharsky, V. K.; Tsokol, A. O. *Rep. Prog. Phys.* **2005**, *68*, 1479.
(4) Brück, E. *J. Phys. D: Appl. Phys.* **2005**, *38*, R381.

(5) Pecharsky, V. K.; Gschneidner, K. A., Jr. *Phys. Rev. Lett.* **1997**, *78*, 4494.
(6) Miller, G. J. *Chem. Soc. Rev.* **2006**, *35*, 799.
(7) Kripyakevich, P. I.; Zarechnyuk, O. S.; Gladyshevskii, E. I.; Bodak, O. I. *Z. Anorg. Allg. Chem.* **1968**, *358*, 90.

from ca. 198 to 262 K while the saturation magnetic moment drops from 2.08 to 1.85 μ_B/Fe.[3,8] Later investigations reported a large volume change (ca. 1.5%) in $LaFe_{11.44}Si_{1.56}$ (reported as $La(Fe_{0.88}Si_{0.12})_{13}$) just above its T_C that was assigned to an itinerant electron metamagnetic (IEM) transition,[9,10] which is defined as a field-induced magnetic transition from the paramagnetic state to the ferromagnetic state above the corresponding Curie temperature.[11] On the basis of these results, a giant MCE was discovered for $LaFe_{11.4}Si_{1.6}$ near its magnetic ordering temperature of 208 K ($\Delta S_M = -11.5$ J/mol·K for $\Delta H = 2$ T).[12] However, as Si further replaces Fe in $LaFe_{13-x}Si_x$, the MCE drops significantly, e.g., in $LaFe_{10.6}Si_{2.4}$, $T_C = 242$ K and $\Delta S_M = -2.5$ J/mol·K for $\Delta H = 2$ T.[13] Since these discoveries, the MCE and magnetic transitions in $LaFe_{13-x}Si_x$ and related phases have been intensively studied,[14-17] but a deeper fundamental understanding of their phase behavior, especially near T_C, is needed.

$LaFe_{13-x}Si_x$ belong to the family of compounds adopting the $NaZn_{13}$-type structure, $RT_{13-x}M_x$ (R = rare-earth element, typically La or Ce; T = Fe, Co, Ni; M = Al, Ga or Si).[18] Both electronic and size factors influence their formation: the coordination environment of the R atom is a 24-vertex snub cube that often requires the larger rare-earth elements, and the $[T_{13-x}M_x]$ network adjusts its composition to optimize chemical bonding.[19] Furthermore, the $NaZn_{13}$-type structure offers numerous possibilities for the distribution of Fe and Si atoms within the network, which is an example of the "coloring problem".[20] The complex interplay among chemical composition, crystal structure, and possible atomic site distributions with electronic and magnetic properties stated above for $LaFe_{13-x}Si_x$ imply a strong influence of orbital interactions on their behavior.

To the best of our knowledge, all of the experimental studies to date on $LaFe_{13-x}Si_x$ are based on polycrystalline samples, and many have contained various impurities, e.g., α-Fe or β-FeSi$_2$.[13,21-23] Furthermore, the literature is scattered with individual reports on specific characteristics for distinct compounds. Therefore, to better understand the relationships among compositions, phase widths, atomic distributions, and electronic structures of these compounds, we have carried out comprehensive structural and theoretical investigations based on single crystalline specimens, with the specific goals of (1) elucidating the effects of a third element on stabilizing the structure and controlling the transformation of cubic $NaZn_{13}$-type structures to the tetragonal derivative and (2) analyzing the electronic structure of $LaFe_{13-x}Si_x$ systems to probe structure−property−bonding relationships.

Experimental Section

Synthesis. $LaFe_{13-x}Si_x$ ($1 \leq x \leq 9$) samples, each with a total mass of ca. 0.5 g, were prepared by arc-melting the stoichiometric quantities of the elements on a water-cooled copper hearth using a tungsten electrode under a high-purity argon atmosphere. The starting materials (La rod, Ames Lab Rare-Earth Metals Preparation Center, 99.0%; Fe chips (Aldrich, 99.98%); Si pieces, Aldrich, 99.5%) were pre-arc-melted to remove impurities such as oxygen on the surface of the elements. During the arc-melting procedure, a titanium or zirconium pellet was heated prior to melting the reactant mixture to further purify the argon atmosphere. The samples were remelted after turning several times to promote sample homogeneity, and weight losses during the arc-melting process were found to be less than 1−2 wt %. The samples obtained were then wrapped in Ta foil (0.025 mm, Aesar, 99.8%), sealed in evacuated fused silica capsules, and annealed at 1273 K for 30 days and subsequently slowly cooled (about 80 K/h) to room temperature. All samples show small amounts of decomposition products after extended exposure to air.

Chemical Analysis. Chemical compositions of $LaFe_{13-x}Si_x$ ($1 \leq x \leq 9$) samples were analyzed by energy dispersive spectroscopy (EDS) quantitative analysis using a JEOL 8400A scanning electron microscope, equipped with an IXRF Systems iridium X-ray analyzer; the resulting compositions complemented the results from single-crystal X-ray analysis. To acquire flat, microscopically smooth surfaces, each sample was polished by sandpaper and fine leather and subsequently inspected by back-scattering and topological modes to determine the sites for elemental analysis. Typical data collections utilized a 20 kV accelerating voltage and a 30 nA beam current. To carry out both quantitative and qualitative analyses, stoichiometric LaNi$_5$ and the pure Fe and Si elements were used as standards.

X-ray Diffraction Studies. Phase analysis was performed by X-ray powder diffraction (XRD) at room temperature and the crystal structures were confirmed by single-crystal X-ray diffraction. Temperature-dependent single-crystal X-ray diffraction was employed to obtain accurate atomic positions, interatomic distances, and elemental distributions across magnetic transitions in selected samples.

Powder X-ray Diffraction Studies. XRD patterns of the samples were obtained with a Huber image plate camera and monochromatic Cu Kα$_1$ radiation ($\lambda = 1.540598$ Å) at ambient temperature (ca. 295 ± 2 K). Powdered samples were homogeneously dispersed on a Mylar film with the aid of a little petroleum jelly. The step size was set at 0.005°, and the exposure time was 1 h. Data acquisition was controlled via the in-situ program. Lattice parameters were obtained from least-squares refinement with the aid of a *Rietveld* refinement program.[24]

Room-Temperature Single-Crystal X-ray Diffraction Studies. Blocklike crystals (typical crystal dimensions: 0.1−0.2 × 0.1−

(8) Palstra, T. T. M.; Mydosh, J. A.; Nieuwenhuys, G. J., van der Kraan, A. M.; Buschow, K. H. J. *J. Magn. Magn. Mater.* **1983**, *36*, 290.
(9) Fujita, A.; Akamatsu, Y.; Fukamichi, K. *J. Appl. Phys.* **1999**, *85*, 4756.
(10) Fujita, A.; Fukamichi, K. *IEEE Trans. Magn.* **1999**, *35*, 3796.
(11) Wohlfarth, E. P.; Rhodes, P. *Philos. Mag.* **1962**, *7*, 1817.
(12) Hu, F. X.; Shen, B. G.; Sun, J. R.; Cheng, Z. H.; Rao, G. H.; Zhang, X. X. *Appl. Phys. Lett.* **2001**, *78*, 3675.
(13) Zhang, X. X.; Wen, G. H.; Wang, F. W.; Wang, W. H.; Yu, C. H.; Wu, G. H. *Appl. Phys. Lett.* **2000**, *77*, 3072.
(14) Fujita, A.; Fujieda, S.; Fukamichi, K. *Phys. Rev.* **2001**, *B65*, 014410.
(15) Fujieda, S.; Fujita, A.; Fukamichi, K. *Appl. Phys. Lett.* **2002**, *81*, 1276.
(16) Wen, G. H.; Zheng, R. K.; Zhang, X. X.; Wang, W. H.; Chen, J. L.; Wu, G. H. *J. Appl. Phys.* **2002**, *91*, 8537.
(17) Hu, F.-X.; Ilyn, M.; Tishin, A. M.; Sun, J. R.; Wang, G. J.; Chen, Y. F.; Wang, F.; Cheng, Z. H.; Shen, B. G. *J. Appl. Phys.* **2003**, *93*, 5503.
(18) Villars, P. *Pearson's Handbook of Intermetallic Phases*; American Society of Metals; Metals Park, OH, 1991.
(19) Pearson, W. B. *Crystal Chemistry and Physics of Metals and Alloys*; Wiley-Interscience: New York, 1972.
(20) Miller, G. J. *Eur. J. Inorg. Chem.* **1998**, *5*, 523.
(21) Sakurada, S.; Tsutai, A.; Sahashi, M. *J. Alloys. Compds.* **1992**, *187*, 67.
(22) Chang, H.; Chen, N.; Liang, J.; Rao, G. *J. Phys. Condens. Matter* **2003**, *15*, 109.
(23) Tang, W.; Liang, J.; Chen, X.; Rao, G. *J. Appl. Phys.* **1994**, *76*, 4095.
(24) Hunter, B. A.; Howard, C. J. *Rietica*; Australian Nuclear Science and Technology Organization: Menai, Australia, 2000.

0.2 × 0.1−0.3 mm³) suitable for structure determination were selected from the products and mounted on glass fibers. Data were collected using a Bruker APEX diffractometer at 295 ± 2 K with monochromated Mo Kα_1 radiation ($\lambda = 0.71073$ Å) and a detector-to-crystal distance of 5.990 cm. Diffraction data were collected in a hemisphere or full sphere of reciprocal space with 0.3° scans in ω for an exposure time of 10 s per frame up to $2\theta = 56.55°$. Intensities were extracted and then corrected for Lorentz and polarization effects using the SAINT program.[25] The program SADABS was used for empirical absorption correction.[26] Structure refinements (full-matrix least-squares on F^2) were performed by using the SHELXTL-PLUS programs.[27]

Low-Temperature Single-Crystal X-ray Diffraction Studies. Data below ambient temperatures were obtained using a Bruker SMART 1000 diffractometer with Mo Kα radiation ($\lambda = 0.71073$ Å). During the low-temperature experiments the temperature was stable within ±1 °C with respect to the value set for an experiment. Data collections and their refinements followed the same procedures as the room-temperature ones.

Electronic Structure Calculations. The theoretical electronic structures of model and actual LaFe$_{13-x}$Si$_x$ structures were calculated self-consistently by the tight-binding linear muffin-tin-orbital (TB-LMTO) method[28−31] within the atomic sphere approximation (ASA) using the LMTO Version 47 program. Exchange and correlation were treated in a local spin density approximation (LSDA).[32] All relativistic effects except spin−orbit coupling were taken into account using a scalar relativistic approximation.[33] Within the ASA, space is filled with overlapping Wigner−Seitz (WS) atomic spheres. The radii of the WS spheres were obtained by requiring the overlapping potential to be the best possible approximation to the full potential according to an automatic procedure.[34] The WS radii for the atomic sites determined by this procedure are in the ranges 2.35−2.39 Å for La, 1.32−1.44 Å for Fe, and 1.36 Å for Si. The basis set included 6s, 6p, 5d, and 4f orbitals for La; 3s and 3p orbitals for Si; and 4s, 4p and 3d orbitals for Fe. The reciprocal space integrations to determine the self-consistent charge densities, densities of states (DOS), and crystal orbital Hamilton populations (COHP)[35] were performed by the tetrahedron method[36] using 216 k points in the irreducible wedges of the corresponding Brillouin zones for the models.

To study the site preference of Si atoms in LaFe$_{13-x}$Si$_x$ structures, semiempirical, Extended Hückel[37−40] (EHT) calculations were performed on molecular [Fe$_{13-n}$Si$_n$]³⁻ ($n = 1-5$) clusters extracted from these structures. These clusters contained various numbers and arrangements of Si atoms; La atoms were treated as donating three valence electrons to each cluster. In EHT, the atomic orbitals

are expressed as Slater-type orbitals: single-ζ functions for Si and double-ζ functions for Fe. All atomic orbital overlaps are calculated within each cluster. Diagonal Hamiltonian matrix elements are given by valence state orbital energies derived from atomic spectra; off-diagonal Hamiltonian matrix elements are approximated by the weighted Wolfsberg−Helmholz approximation.[40] Total energies are calculated by summing the occupied molecular orbital energies. The atomic parameters are Fe 4s, $H_{ii} = -9.22$ eV, $\zeta_1 = 1.90$; Fe 4p, $H_{ii} = -5.37$ eV, $\zeta_1 = 1.90$; Fe 3d, $H_{ii} = -12.28$ eV, $\zeta_1 = 5.55$, $c_1 = 0.5411$, $\zeta_1 = 1.80$, $c_1 = 0.6734$; Si 3s, $H_{ii} = -17.3$ eV, $\zeta_1 = 1.63$; Si 3p, $H_{ii} = -9.20$ eV, $\zeta_1 = 1.43$.

Results and Discussion

Phase Behavior of LaFe$_{13-x}$Si$_x$. Several different samples with loaded compositions LaFe$_{13-x}$Si$_x$ ($1 \leq x \leq 9$) were studied by EDS and XRD. According to our synthetic procedures, cubic or tetragonally distorted NaZn$_{13}$-type phases were observed for samples loaded in the range $1 \leq x < 6$. The Si-rich mixtures ($x \geq 6$) gave LaFe$_2$Si$_2$[41] as the major product with additional amounts of FeSi[42] and trace amounts of a tetragonally distorted NaZn$_{13}$-type phase. In the Fe-rich mixtures ($1 \leq x < 6$), small amounts of α-Fe, FeSi, or LaFe$_2$Si$_2$ as impurity phases could occasionally be observed in both EDS and X-ray powder diffraction patterns. For the $x = 6$ sample, EDS analysis suggested and the refined lattice parameters confirmed a phase closer to "LaFe$_8$Si$_5$" than "LaFe$_7$Si$_6$". The results of phase analysis are summarized in Supporting Information, Table S1.

Figure 1a illustrates the powder XRD patterns at ca. 298 K for LaFe$_{13-x}$Si$_x$ for the loaded range $1 \leq x \leq 5$. In the range $1 \leq x \leq 2.8$, LaFe$_{13-x}$Si$_x$ show single-phase, cubic NaZn$_{13}$-type structures, space group $Fm\bar{3}c$. Neither EDS nor single-crystal X-ray diffraction refinements confirmed the existence of "LaFe$_{12}$Si"; the lowest concentration of Si we could ascertain was ca. $x = 1.3$, which agrees with earlier assessments.[14,15] For the $x = 3$ and 3.2 samples, XRD showed that the cubic NaZn$_{13}$ phase coexists with a tetragonally distorted phase. For the range $3.2 < x \leq 5$, the XRD patterns could be successfully indexed with a body-centered tetragonal cell, which is based on a distortion of the cubic NaZn$_{13}$-type unit cell, i.e., the Ce$_2$Ni$_{17}$Si$_9$ structure type, space group I4/mcm.[43] An example of how the diffraction patterns in the 2θ range 24−33° for the two unit cells compare is shown in Figure 1b. Thus, we conclude that the range of composition for the existence of NaZn$_{13}$-related phases in LaFe$_{13-x}$Si$_x$ is $1.3(1) \leq x \leq 5.0(1)$ and that there is a coexistence range of $2.7(1) \leq x \leq 3.3(1)$ between a cubic structure at lower Si concentrations and a tetragonal structure at higher Si concentrations.

Figure 2 illustrates the concentration dependence of the lattice parameters on the Si content in LaFe$_{13-x}$Si$_x$ compounds. The results of both single-crystal and powder X-ray diffraction are shown. Since the relationship between the tetragonal unit cell and the cubic unit cell is approximately $a_{\text{tet}} \cong a_{\text{cub}}/\sqrt{2}$ and $c_{\text{tet}} \cong c_{\text{cub}}$, we plot $\sqrt{2}a_{\text{tet}}$ to show an

(25) *SAINT*; Bruker AXS, Inc.: Madison, WI, 1996.
(26) Blessing, R. H. *Acta. Crystallogr.* **1995**, *A51*, 33.
(27) *SHELXTL-Plus*; Bruker AXS, Inc.: Madison, WI.
(28) Andersen, O. K. *Phys. Rev.* **1975**, *B12*, 3060.
(29) Andersen, O. K.; Jepsen, O. *Phys. Rev. Lett.* **1984**, *53*, 2571.
(30) Andersen, O. K.; Jepsen, O.; Glötzel, D. In *Highlights of Condensed-Matter Theory*; Bassani, F., Fumi, F., Tosi, M. P., Lambrecht, W. R. L., Eds.; North-Holland: New York, 1985.
(31) Andersen, O. K. *Phys. Rev.* **1986**, *B34*, 2439.
(32) Von Barth, U.; Hedin, L. *J. Phys. C* **1972**, *5*, 1629.
(33) Koelling, D. D.; Harmon, B.N. *J. Phys. C* **1977**, *10*, 3107.
(34) Jepsen, O.; Andersen, O. K. *Z. Phys. B* **1995**, *97*, 645.
(35) Dronskowski, R.; Blöchl, P. *J. Phys. Chem.* **1993**, *97*, 8617.
(36) Blöchl, P. E.; Jepsen, O.; Andersen, O.K. *Phys Rev.* **1994**, *B49*, 16223.
(37) Hoffmann R. *Solids and Surfaces: A Chemist's View of Bonding in Extended Structures*; VCH: New York, 1988.
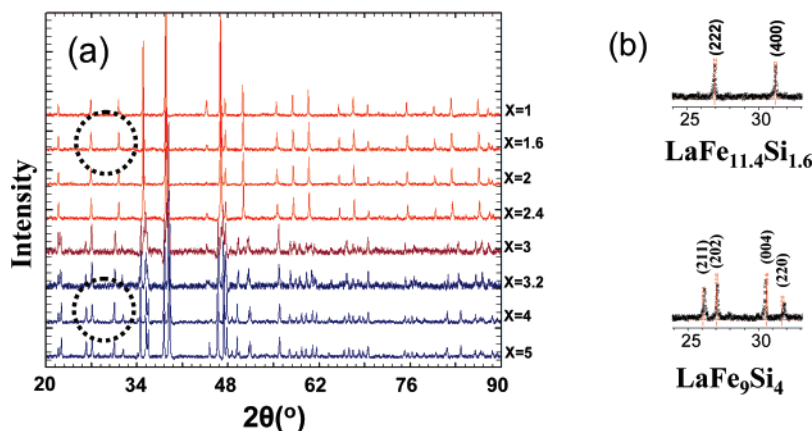(38) Hoffmann, R. *J. Chem. Phys.* **1963**, *39*, 1397.
(39) Burdett, J. K. *Chemical Bonding in Solids*; Oxford University Press: New York, 1995.
(40) Ammeter, J. H.; Bürgi, H. -B; Thibeault, J. C.; Hoffmann, R. *J. Am. Chem. Soc.* **1978**, *100*, 3686.
(41) Rossi, D.; Marazza, R.; Ferro, R. *J. Less-Common Met.* **1978**, *58*, 203.
(42) Neshpor, V. S. *Kristallografiya* **1961**, *6*, 466.
(43) Bodak, O. I. *Kristallografiya* **1979**, *24*, 1280.

Figure 1. (a) XRD powder patterns of LaFe$_{13-x}$Si$_x$ (1 ≤ x ≤ 5) taken at room temperature using Cu Kα radiation for the 2θ range 20−90°. Red curves are for single-phase, cubic structures; blue curves are for single-phase, tetragonal structures. Loaded compositions are noted next to each pattern. (b) Indexed XRD powder patterns of cubic LaFe$_{11.4}$Si$_{1.6}$ and tetragonal LaFe$_9$Si$_4$ in the 2θ range 24−34° after annealing at 1000 °C.
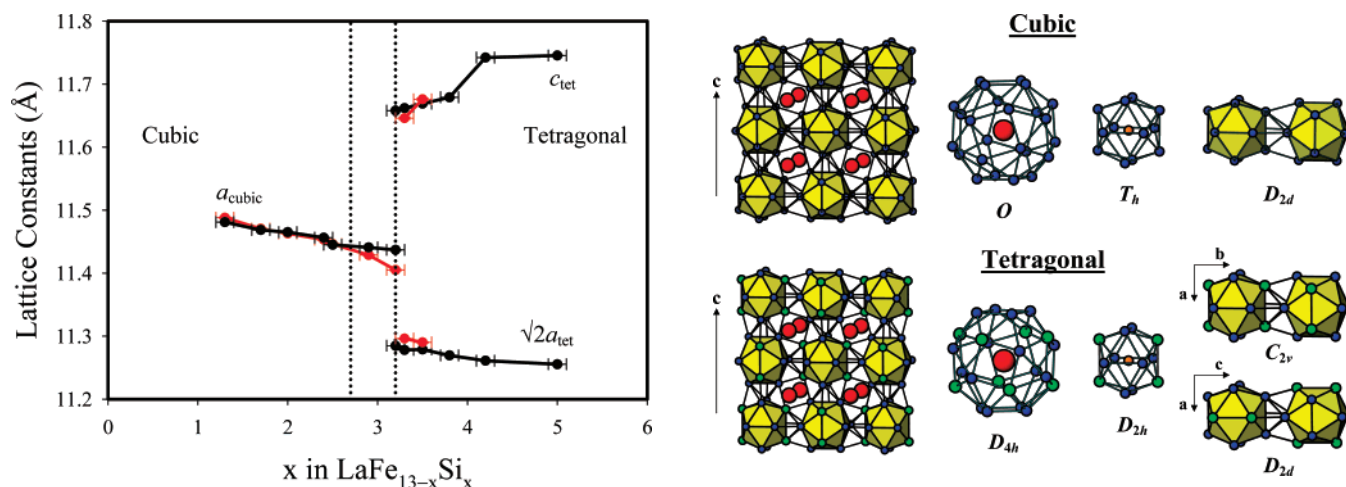
Figure 2. Concentration dependence of the unit cell parameters in LaFe$_{13-x}$Si$_x$ at room temperature. For comparison between the two crystal classes, $\sqrt{2}a_{tet}$ is plotted for the tetragonal phases. Black curves are from powder diffraction data; red curves are from single-crystal diffraction data.

Figure 3. (001) projections and coordination polyhedra in cubic and tetragonal LaFe$_{13-x}$Si$_x$ structures. Red circles, La; orange circles, Fe(I); blue circles, Fe(II); green circles, Si. The site symmetry for each coordination polyhedron is noted.

immediate comparison between the two phases. The lattice parameters, as well as volumes per formula unit, of LaFe$_{13-x}$Si$_x$ (1.3(1) ≤ x ≤ 5.0(1)) decrease with Si concentration, which is consistent with the covalent radii of Fe (1.25 Å) and Si (1.18 Å).[44] Furthermore, the Si-rich, tetragonal phases show elongation along the c axis with respect to the a and b axes. In general, we observe excellent agreement between values obtained by powder and single-crystal X-ray diffraction.

Room-Temperature Crystal Structures of LaFe$_{13-x}$Si$_x$. The crystallographic data, atomic positions and site occupancies, and significant interatomic distances for LaFe$_{13-x}$Si$_x$ (1 < x < 6) determined by single-crystal X-ray diffraction at 298 K are summarized in the Supporting Information, Tables S2−S4. The cubic and tetragonal structures of these phases, shown as (001) slices in Figure 3, involve a simple cubic packing (or nearly so, in the case of the tetragonal structures) of atom-centered [Fe$_{13-x}$Si$_x$] icosahedra with La atoms in the interstices. Refinements in all cases place Fe(I) atoms at the centers of the [Fe$_{13-x}$Si$_x$] icosahedra, so we formulate

these clusters as [Fe(Fe$_{12-x}$Si$_x$)] and the compounds as La[Fe(Fe$_{12-x}$Si$_x$)]. Furthermore, in the cubic structures (space group $Fm\bar{3}c$), Si and Fe are randomly distributed among the icosahedral Fe(II)/Si (96i) sites, whereas Si preferentially occupies one set of 16l sites in the tetragonal structures (space group I4/mcm). The Fe-centered icosahedra contradict conclusions, based on neutron powder diffraction of the cubic phases, which reported that Si atoms randomly substituted for Fe atoms on the two different sites,[37] but agrees with a recent Mössbauer spectroscopic evaluation of La(Fe$_{0.81}$Si$_{0.19}$)$_{13}$.[45] Although the nuclear elastic scattering factors for Fe and Si are distinctly different (9.54 and 4.15 fm, respectively), various factors affecting the intensities of powder diffraction patterns could influence the refinement of these occupancies.

Figure 3 also illustrates the three polyhedra making up these structures: (1) the "snub cube" arrangement of 24 Fe-(II)/Si atoms surrounding each La atom, (2) the Fe-centered icosahedron, and (3) the eight-vertex stella quadrangula

(44) Huheey, J. E.; Keiter, E. A.; Keither, R. L. *Inorganic Chemistry: Principles of Structure and Reactivity*, 4th ed.; Harper Collins College Publishers: New York, 1993; pp 292.

(45) Hamdeh, H. H.; Al-Ghanem, H.; Hikal, W. M.; Taher, S. M.; Ho, J. C.; Anh, D. T. K.; Thuy, N. P.; Duc, N. H.; Thang, P. D. *J. Magn. Magn. Mater.* **2004**, *269*, 404.

bridging two adjacent icosahedra, which creates a central tetrahedron with each face capped by an additional atom to give four tetrahedra fused to the central one. The snub cube will effectively encapsulate larger atoms like La. In the cubic phases, its site symmetry is O (432) but lowers to D_4 (422) in the tetragonal structures. Therefore, as the Si concentration increases, 24 equal La−Fe(II)/Si distances segregate into three distinct sets of distances. Moreover, at the lower limit of Si content ($x = 1.3$), randomly distributed Si atoms gives, on average, 2.6 Si atoms coordinated to every La atom, i.e., each La atom is in close contact with two to three Si atoms throughout the structure. At the upper limit of Si content for the cubic phases ($x = 2.8$), randomly distributed Si atoms would give, on average, 5.6 Si atoms coordinated to every La atom. However, in the tetragonal structures, there are eight Si-preferred sites close to each La atom. The Fe-centered icosahedra also show a symmetry lowering from T_h ($m\bar{3}$) to D_{2h} (mmm) as the Si content increases, so that 12 equivalent Fe(I)−Fe(II)/Si contacts separate into three sets of four different Fe(I)−Fe(II) and Fe(I)−Si distances. However, in all cases, these icosahedra are far from regular because the Fe(II)/Si positions create two distinct sets of intra-icosahedral distances. Finally, in the cubic structures, all stella quadrangulae are equivalent, point symmetry D_{2d} ($\bar{4}m2$), but become inequivalent in the tetragonal structures: within the *ab* planes, the point symmetry is C_{2v} ($m2m$) with a central [Fe$_2$Si$_2$] tetrahedron fused with four [Fe$_3$Si] tetrahedra, and within the *ac* and *bc* planes, the point symmetry is D_{2d} ($\bar{4}2m$) with a central [Fe$_4$] tetrahedron fused with four [Fe$_3$Si] tetrahedra. Thus, the transformation from cubic to tetragonal crystal classes is strongly influenced by the distribution of Fe and Si atoms and the secondary effect on the $c/\sqrt{2}a$ ratio in the tetragonal phases is determined by the interactions between Fe-centered icosahedra.

Distance Analysis of the Structural Transformation. As seen in Figure 2, the lattice parameters and, therefore, volumes decrease as the Si content increases in La[Fe(Fe$_{12−x}$Si$_x$)]. Thus, we expect the interatomic distances to show similar trends (see Supporting Information, Table S4). Figure 4 plots the changes in significant distances, which are categorized according to the polyhedral analysis in the previous section: intra-icosahedral Fe(II)/Si−Fe(II)/Si (a) and (b); inter-icosahedral Fe(II)/Si−Fe(II)/Si (c) and (d); Fe(I)−Fe(II)/Si (e); and La−Fe(II)/Si (f). Among the cubic phases, the Fe-(I)−Fe(II) distances (e) are one of the two shortest contacts (ca. 2.45 Å) and they decrease slightly by 0.45% with increasing Si concentration, while the La−Fe(II)/Si distances (f) are the longest (ca. 3.33 Å) and show 0.89% contraction. For the remaining distances, those *between* icosahedra are distinctly shorter than those *within* icosahedra. The Fe(II)/Si−Fe(II)/Si contact (d) is the shortest distance (ca. 2.44 Å) and exhibits the most pronounced reduction (ca. 1.39%) with increasing Si content, whereas contact (c) remains nearly constant at ca. 2.50(1) Å. Among the two intra-icosahedral distances, the longer one (b) (ca. 2.69 Å) increases slightly, whereas, the shorter distance (a) (ca. 2.55 Å) decreases by 0.63%. As the Si content increases, contact (b) transforms from mostly Fe−Si to Si−Si interactions.
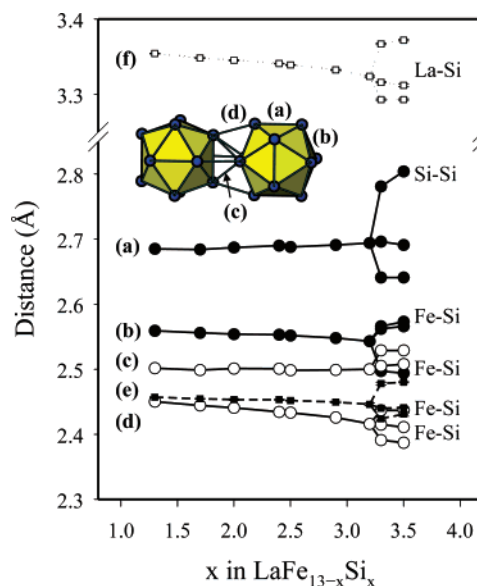
Figure 4. Concentration dependence of the interatomic distances in LaFe$_{13−x}$Si$_x$ at room temperature. Filled circles are intra-icosahedral contacts **a** and **b**; open circles are inter-icosahedral contacts **c** and **d**; filled squares are Fe(I)−Fe(II)/Si contacts **e**; open squares are La−Fe(II)/Si contacts **f**.

For the tetragonal structure, all bond lengths separate into three distinct sets with intra-icosahedral contacts (a) and (b) showing greater splitting than the inter-icosahedral contacts (c) and (d). Due to the segregation of Fe and Si atoms among the icosahedral sites, the Si−Si intra-icosahedral contact increases by over 0.1 Å. Furthermore, the shortest inter-icosahedral contact is a Fe−Fe pair with a distance close to 2.40 Å. In general, further increase in Si concentration would lead to shorter La−Fe contacts and an increased concentration of Si−Si contacts, both of which show repulsive character: (i) a repulsive La−Fe interatomic potential leads to the positive ΔH_f^0 for "LaFe$_{13}$"[23] and (ii) the Si−Si contacts show a distinct increase in distance.

Figure 2 indicates that the distortion to the tetragonal structure appears as a contraction along the cubic *a* and *b* axes relative to the *c* axis, and Figure 4 emphasizes that the distances within the stella quadrangulae are more affected by this transformation than those within the icosahedra. On the basis of the atomic distributions in the tetragonal phases, for La[Fe(Fe$_8$Si$_4$)], the stella quadrangulae in the *ab* plane have six Fe(II)−Si and two Fe(II)−Fe(II) inter-icosahedral contacts, while those in the *ac* and *bc* planes have four Fe(II)−Si and four Fe(II)−Fe(II) contacts. Thus, there are more Fe(II)−Fe(II) interactions along the *c* direction than in either the *a* or *b* directions. Figure 5 illustrates COHP curves for these two different sets of pairwise orbital interactions for LaFe$_9$Si$_4$. As seen in these curves, the Fe-(II)−Si orbital interactions are nearly optimized at the corresponding Fermi level with no Fe(II)−Si antibonding states occupied, whereas the Fe(II)−Fe(II) contact shows some antibonding character at the Fermi level. Thus, the population analysis of the electronic structure of LaFe$_9$Si$_4$ confirms the observed lattice distortions in the tetragonal phases.
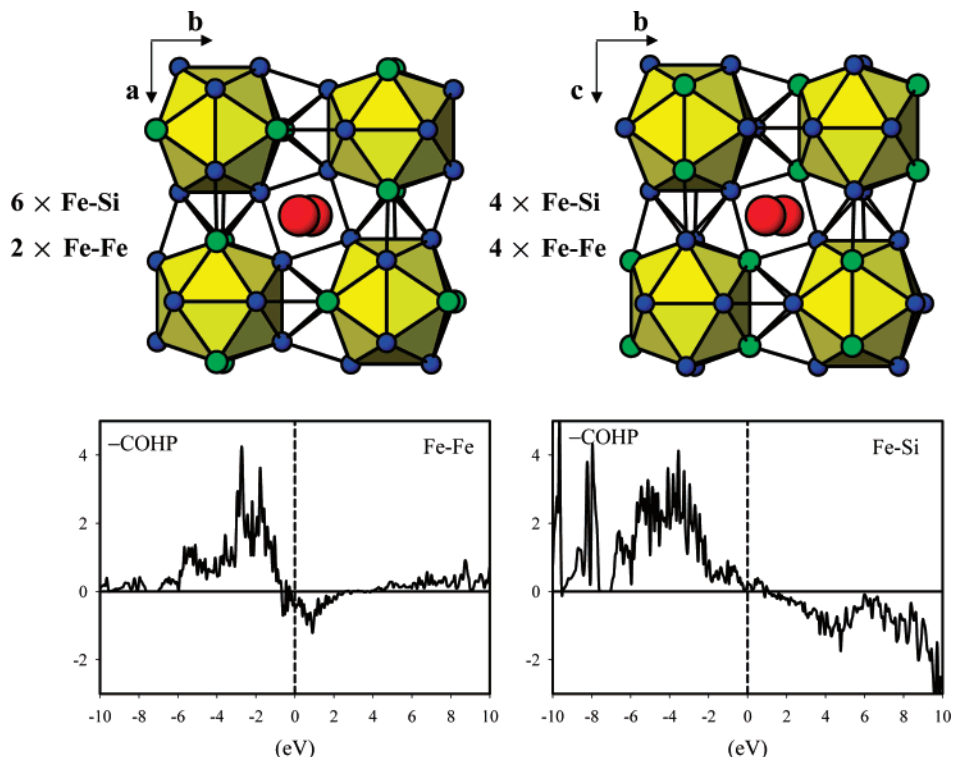
Figure 5. COHP curves for inter-icosahedral Fe−Fe and Fe−Si contacts found in LaFe$_9$Si$_4$. (001) and (100) projections are illustrated, left and right, respectively, to emphasize the different inter-icosahedral environments. In the COHP curves, the Fermi level is set at 0 eV, noted by the dashed line. Bonding states: −COHP > 0; antibonding states: −COHP < 0.

Ordering of Fe and Si Atoms. According to all accounts, ternary R[T$_{13-x}$M$_x$] phases show M elements randomly occupying the icosahedral (96i) sites in the cubic structures, but then preferential occupation of one set of sites (16l) in the tetragonal Ce$_2$Ni$_{17}$Si$_9$-type structures, and La[Fe(Fe$_{12-x}$Si$_x$)] is no exception. What controls this pattern? Although we can describe the NaZn$_{13}$-type structure as a CsCl-type packing of atom-centered icosahedra with large "cations," our distance analysis for La[Fe(Fe$_{12-x}$Si$_x$)] suggests that the influential polyhedra are the stella quadrangulae between icosahedra. Nevertheless, to examine the question of site preferences for Fe and Si atoms in these phases initially, we have used the Fe-centered icosahedron as the basic building block of the La[Fe(Fe$_{12-x}$Si$_x$)] structure by constructing the various stereoisomers, or polytypes,[46] for [Fe(Fe$_{12-n}$Si$_n$)] and calculating the molecular orbital energy for each [Fe(Fe$_{12-n}$Si$_n$)]$^{3-}$ within EHT. In this model, we assume that La donates its complement of valence electrons to the more electronegative elements.

As the number of Si atoms increases, the number of different stereoisomers increases rapidly. The enumeration of all possible stereoisomers for centered or noncentered icosahedra has been thoroughly discussed using Pólya's theorem.[47−50] Figure 6 shows all possible stereoisomers of

the icosahedra [Fe(Fe$_{12-n}$Si$_n$)] for $n = 1-4$ and the relative molecular orbital energies of [Fe(Fe$_{12-n}$Si$_n$)]$^{3-}$ (with respect to the lowest energy stereoisomer for each n). A previous analysis on [Cu(Cu$_4$Al$_8$)]$^{2-}$ clusters found in BaCu$_5$Al$_8$ pointed out a nearly linear relationship between the total molecular orbital energy and the number of homoatomic contacts within the stereoisomers of the [Cu(Cu$_4$Al$_8$)]$^{2-}$ icosahedra.[51] We reproduce this graph in Figure 7 and add the corresponding results for the [Fe(Fe$_8$Si$_4$)]$^{3-}$ clusters— again we see a linear relationship, but the slope of the line is higher in the Fe/Si case than for the Cu/Al case. According to these calculations, the most stable stereoisomers are those with the fewest number of homoatomic Si−Si contacts.

In general, the clusters with the lowest molecular orbital energies should be the most thermodynamically stable and accessible. According to Figure 6b, the energy differences between the lowest energy configurations and higher energy ones increases as the Si content increases. Therefore, under high-temperature synthetic conditions, the configurational entropy associated with random distributions of Si atoms will contribute to stabilizing the cubic structure for LaFe$_{11}$Si$_2$ and LaFe$_{10}$Si$_3$, i.e., examples with low Si content, while enthalpic reasons favor an ordering of Si atoms at higher concentrations, as in LaFe$_9$Si$_4$. This argument accounts well for the previous results of *cubic* BaCu$_5$Al$_8$ with a random distribution of Cu and Al atoms on the icosahedron due to the smaller energy differences between each stereoisomer[51] and of the

(46) McLarnan, T. J.; Moore, P. B. In *Structure and Bonding in Crystals*; O'Keeffe, M., Navrotsky, A., Eds.; Academic Press: New York, 1981; Vol. II, p 133.
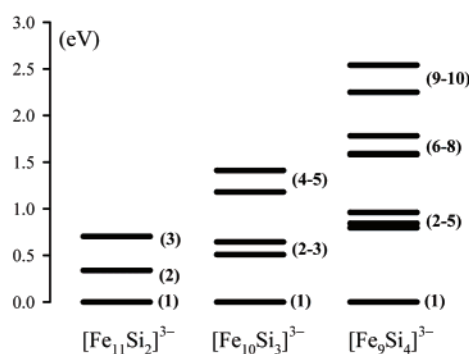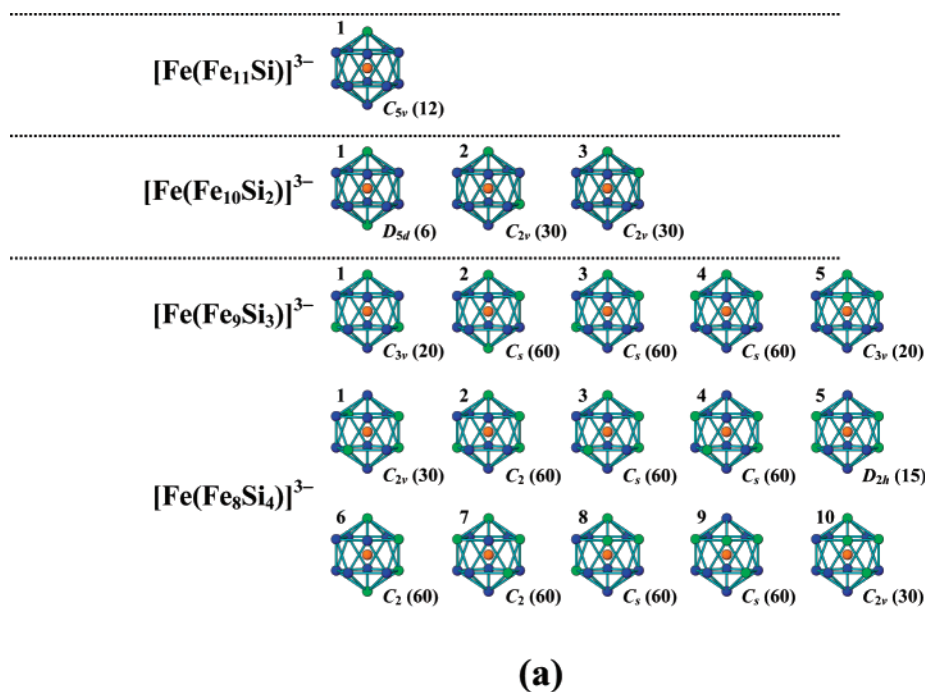(47) Teo, B. K.; Zhang, H.; Kean, Y.; Dang, H.; Shi, X. *J. Chem. Phys.* **1993**, *9*, 2929.
(48) Teo, B. K.; S, A.; Elber, R.; Zhang, H. *Inorg. Chem.* **1998**, *37*, 2482.
(49) McLarnan, T. *J. Solid State Chem.* **1978**, *26*, 235.
(50) Burdett, J. K. *Inorg. Chem.* **1975**, *14*, 375.

(51) Nordell, K. J.; Miller, G. J. *Inorg. Chem.* **1999**, *38*, 579.

(a)

(b)

Figure 6. (a) All possible stereoisomers and point group symmetries of $[Fe(Fe_{12-n}Si_n)]$ ($n = 1, 2, 3, 4$) centered icosahedra. Same color scheme as in Figure 3. Numbers in parentheses following the point group equal the number of stereoisomers. The $[Fe(Fe_{12-n}Si_n)]^{3-}$ clusters are arranged in order of increasing molecular orbital energies. (b) Relative molecular orbital energy values for the different stereoisomers.
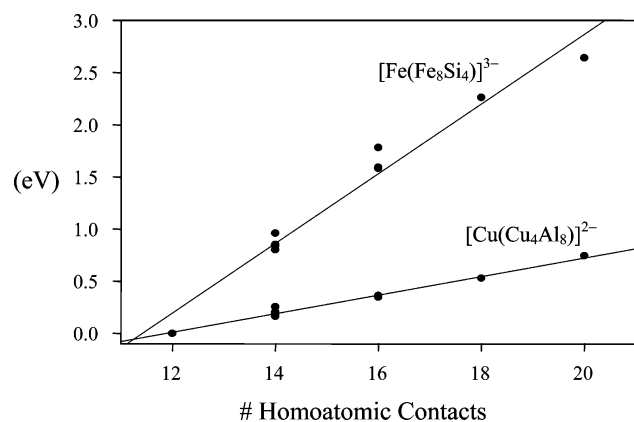

Figure 7. Graphical representation of the relative total energies of $[Fe(Fe_8Si_4)]^{3-}$ and $[Cu(Cu_4Al_8)]^{2-}$ icosahedra vs the number of homoatomic (Fe−Fe, Si−Si; Cu−Cu, Al−Al) contacts in each cluster. For this composition, the minimum number of such contacts in the icosahedron is 12.

structural transformations in $LaFe_7Al_6$ by annealing at low temperature for prolonged times.[52]

We must point out, however, that the lowest energy $[Fe(Fe_8Si_4)]^{3-}$ icosahedral cluster is *not* the one found in $LaFe_9Si_4$. Rather, it is the cluster ranked fifth in the energy sequence. However, our EHT calculations on the icosahedral clusters indicate that the Si atom distribution will be governed by minimizing the number of close Si−Si contacts *throughout the entire three-dimensional structure*. Therefore, we carried out calculations on full three-dimensional (3-D) structures of tetragonal $LaFe_9Si_4$ using several different arrangements of atoms in these clusters. Examples of these models are shown in Figure 8: model (A) has Si atoms on the $16l(1)$ sites, model (B) has Si atoms on the $16l(2)$ sites, and model (C) has Si atoms on the $16k$ sites. The total energies clearly show that arrangement **5** in Figure 6 for $[Fe(Fe_8Si_4)]^{3-}$, i.e., model (B), shows the lowest energy after building the complete 3-D structure and is entirely consistent with the concept of minimizing the number of short Si−Si

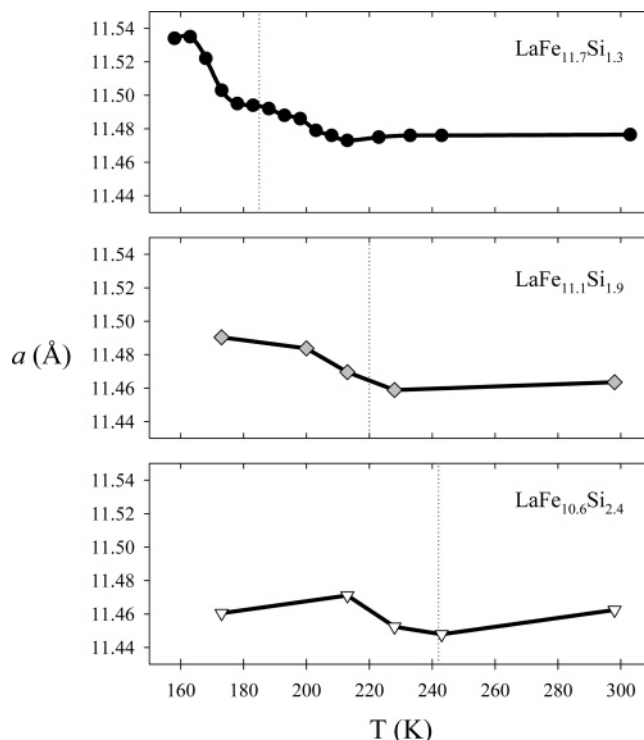(52) Weihua, T.; Jingkui, L. *Phys. Rev.* **1994**, *B49*, 49.
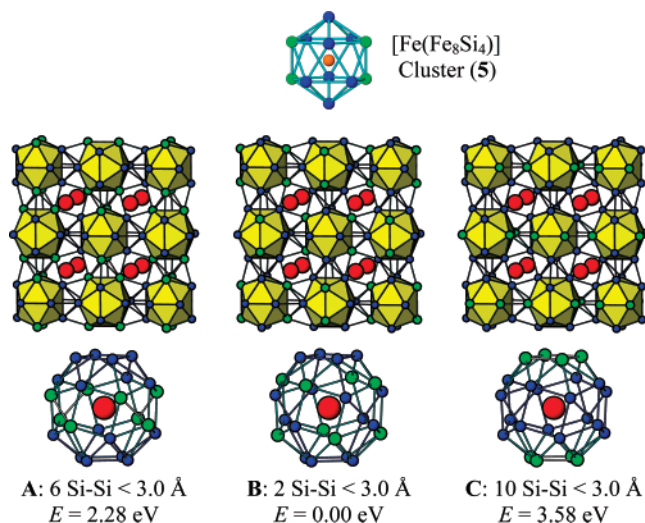
Figure 8. Three different structural models of $LaFe_9Si_4$ studied by electronic structure calculations to explore the "coloring problem". All three models are based on the $[Fe(Fe_8Si_4)]$ icosahedron shown at the top. Si−Si contact analysis in the snub cube coordination surrounding each La site is indicated, as well as the relative total energy per formula unit for each model.

Figure 9. Temperature dependence of the lattice parameters for $LaFe_{11.7(1)}$-$Si_{1.3(1)}$, $LaFe_{11.1(1)}Si_{1.9(1)}$, and $LaFe_{10.6(1)}Si_{2.4(1)}$ as obtained from single-crystal X-ray diffraction experiments. The corresponding Curie temperature for each compound is indicated by dotted lines.

contacts (or, equivalently, maximizing the separation between Si atoms) in these $La[Fe(Fe_{12-x}Si_x)]$ structures. The next preferred sites are $16l(1)$, and these should be occupied for Si content exceeding $x = 4$. The $16k$ site is completely avoided.

Temperature-Dependent X-ray Diffraction. An important goal of this work is to use single-crystal X-ray diffraction around the Curie temperatures of the cubic phases to investigate structural details of the magnetic transition. Therefore, data were collected for $LaFe_{11.7(1)}Si_{1.3(1)}$ (T_C = ca. 185 K[14,53]) between 163(1) and 293(1) K, and for $LaFe_{11.1(1)}$-$Si_{1.9(1)}$ (T_C = ca. 220 K), and $LaFe_{10.6(1)}Si_{2.4(1)}$ (T_C = ca. 240 K[16]) from 173(1) to 293(1) K. The temperature dependence of the lattice constants are shown in Figure 9. All samples show an increase in volume on cooling across the corresponding Curie temperatures, which can be assigned to the magnetovolume effect.[54] In the paramagnetic state, there are randomly oriented magnetic moments, and with decreasing temperature, the compound displays a normal volume contraction. Below the Curie temperature, the magnetic moments in the structure align into the ferromagnetic state and create the volume expansion. Further cooling leads to volume contraction. However, near the corresponding T_C values, there are anomalies, as has been observed for other rare-earth transition metal compounds.[55−57]

For $LaFe_{11.7(1)}Si_{1.3(1)}$ the change of unit cell volume occurs abruptly near the magnetic transition reported at ca. 185 K.[14,53] In fact, there is a slight increase in volume at ca. 215

K, an increase that continues gradually until ca. 175 K, at which temperature there is a 1.05% increase in volume on further cooling. This behavior was also observed in powder samples, which showed negative, nonlinear thermal expansion coefficients between 153 and 213 K.[58] Overall, $LaFe_{11.7(1)}$-$Si_{1.3(1)}$ exhibits a volume increase on cooling from room temperature to just below T_C by 1.51%, which implies a possible first-order transition between the low-temperature ferromagnetic phase and the high-temperature paramagnetic phase. These effects have been assigned to an itinerant electron metamagnetic (IEM) transition,[59−62] which can also contribute to giant MCE.[63] In contrast, $LaFe_{11.1(1)}Si_{1.9(1)}$ and $LaFe_{10.6(1)}Si_{2.4(1)}$ show smaller increases of lattice parameters on cooling across their T_C values, resulting in volume expansions, respectively, of 0.83% and 0.66%. The decreasing volume changes across the Curie points with increasing Si content are consistent with the decreasing saturation magnetic moments and MCE in this series of compounds.

Possible Symmetry Reduction around T_C? Many materials showing a giant MCE exhibit a coupling between their magnetic transitions and some kind of structural transformation.[64,65] Thus, it is somewhat surprising that a giant MCE

(53) Wang, F.; Wang, G.; Hu, F.; Kurbakov, A.; Shen, B.; Cheng, Z. *J. Phys.: Condens. Matter* **2003**, *15*, 5269.
(54) *Magnetism: Fundamentals*; du Trémolet de Lacheisserie, É., D. Gignoux, D., Schlenker, M., Eds.; Springer, New York, 2005.
(55) Kamar'ad, J.; Arnold, Z.; Morellon, L.; Algarabel, P. A.; Ibarra, M. R.; Fuerst, C. D. *J. Appl. Phys.* **1996**, *79*, 4656.
(56) Gratz, E.; Hauser, R.; Lindbaum, A.; Maikis, M.; Resel, R.; Schaudy, G.; Levitin, R. Z.; Markosyan, A. S.; Dubenko, I. S.; Sokolov, A. Yu.; Zochowski, S. W. *J. Phys.: Condens. Matter.* **1995**, *7*, 597.
(57) Givord, D.; Lemaire, R. *IEEE Trans. Magn.* **1974**, *10*, 109.

(58) Chang, H.; Liang, J.-K.; Shen, B.-G.; Yang, L.-T.; Wang, F.; Chen, N.-X.; Rao, G.-H. *J. Phys. D* **2003**, *36*, 160.
(59) Saito, H.; Yokoyama, T.; Terada, Y.; Fukamichi, K.; Mitamura, H.; Goto, T. *Solid State Commun.* **2000**, *113*, 447.
(60) Goto, T.; Shindo, Y.; Ogawa, S.; Harada, T. *Physica B* **1997**, *237*, 482.
(61) Yamada, H. *Phys. Rev.* **1993**, *B47*, 11211.
(62) Yamada, H.; Terao, K. *J. Phys.: Condens. Matter* **1994**, *6*, 10805.
(63) Yamada, H.; Goto, T. *Phys. Rev.* **2003**, *B68*, 184417.
(64) Choe, W.; Pecharsky, V. K.; Pecharsky, A. O.; Gschneidner, K. A., Jr.; Young, V. G., Jr.; Miller, G. J. *Phys. Rev. Lett.* **2000**, *84*, 4617.

Table 1. X-ray single-crystal data and structure refinements for $LaFe_{11.7(1)}Si_{1.3(1)}$ and $LaFe_{10.6(1)}Si_{2.4(1)}$ at various temperatures

	$LaFe_{11.7(1)}Si_{1.3(1)}$									
temp	293		243		213		183		173	
a (Å)	11.4727(13)		11.4695(13)		11.4626(13)		11.4680(13)		11.5116(13)	
$2\theta_{max}$ (deg)	56.30		56.32		56.36		56.86		56.10	
index ranges h	−15 to 15		−15 to 15		−15 to 15		−15 to 15		−14 to 14	
k	−15 to 15		−15 to 11		−15 to 11		−15 to 15		−15 to 13	
l	−15 to 15		−15 to 15		−15 to 15		−15 to 11		−15 to 13	
no. reflns	3381		2263		2273		2285		1905	
space group	$Fm\bar{3}c$	$F\bar{4}3c$	$Fm\bar{3}c$	$F\bar{4}3c$	$Fm\bar{3}c$	$F\bar{4}3c$	$Fm\bar{3}c$	$F\bar{4}3c$	$Fm\bar{3}c$	$F\bar{4}3c$
ind. reflns	96	163	96	163	96	163	98	167	96	163
R(int)	0.0479	0.0475	0.0655	0.0648	0.0452	0.0448	0.0695	0.0689	0.0452	0.0442
data/params	96/11	163/14	96/11	163/14	96/11	163/14	98/11	167/14	96/11	163/14
R1 [$I > 2\sigma(I)$]	0.0142	0.0136	0.0159	0.0160	0.0178	0.0179	0.0309	0.0267	0.0269	0.0211
wR2	0.0297	0.0297	0.0436	0.0355	0.0433	0.0399	0.0719	0.0639	0.0769	0.0469
GOF (F^2)	1.216	1.162	1.260	1.261	1.295	1.277	1.384	1.351	1.084	1.310
ext. coeff. ($\times 10^{-4}$)	1.6(5)	1.4(4)	2.2(8)	0.9(4)	1.8(8)	0.9(5)	1.5(12)	0.5(7)	4.7(17)	1.6(6)
abs. structure param		0.6(4)		0.5(5)		0.9(5)		0.8(6)		0.3(4)
$\Delta\rho_{max}$ (e$^-$/Å^3)	0.60	0.46	0.81	0.63	1.50	1.12	1.54	1.04	1.73	0.89
$\Delta\rho_{min}$ (e$^-$/Å^3)	−0.66	−0.47	−0.64	−0.55	−0.62	−1.52	−1.54	−1.14	−1.14	−0.80

	$LaFe_{10.6(1)}Si_{2.4(1)}$									
temp	293		243		228		213		173	
a (Å)	11.4624(13)		11.4479(13)		11.4524(13)		11.4711(13)		11.4605(13)	
$2\theta_{max}$ (deg)	56.36		56.44		56.42		56.32		56.36	
index ranges, h	−13 to 14		−13 to 13		−13 to 13		−15 to 14		−14 to 15	
k	−10 to 14		−15 to 8		−5 to 14		−15 to 12		−15 to 12	
l	−14 to 14		−5 to 14		−15 to 8		−12 to 14		−14 to 12	
no. reflns	1850		1117		1104		1884		1915	
space group	$Fm\bar{3}c$	$F\bar{4}3c$	$Fm\bar{3}c$	$F\bar{4}3c$	$Fm\bar{3}c$	$F\bar{4}3c$	$Fm\bar{3}c$	$F\bar{4}3c$	$Fm\bar{3}c$	$F\bar{4}3c$
ind. reflns	95	159	94	158	94	158	95	161	95	161
R(int)	0.0309	0.0305	0.0436	0.0426	0.0379	0.0358	0.0375	0.0371	0.0377	0.0373
data/params	95/11	159/14	94/11	158/14	94/11	158/14	95/11	161/14	95/11	161/14
R1 [$I > 2\sigma(I)$]	0.0109	0.0102	0.0183	0.0172	0.0198	0.0205	0.0136	0.0129	0.0107	0.0101
wR2	0.0243	0.0243	0.0469	0.0423	0.0456	0.0439	0.0314	0.0293	0.0259	0.0256
GOF (F^2)	1.265	1.261	1.550	1.369	1.547	1.375	1.307	1.305	1.347	1.271
ext. coeff. ($\times 10^{-4}$)	3.8(5)	3.5(4)	4.2(9)	3.2(6)	3.6(9)	2.8(6)	4.0(7)	3.4(5)	3.3(5)	3.1(4)
abs. structure param		0.6(3)		0.8(3)		0.5(4)		0.4(3)		0.5(4)
$\Delta\rho_{max}$ (e$^-$/Å^3)	0.48	0.52	0.65	0.60	0.67	0.75	0.53	0.32	0.30	0.38
$\Delta\rho_{min}$ (e$^-$/Å^3)	−0.34	−0.34	−0.58	−0.58	−0.65	−0.55	−0.43	−0.49	−0.45	−0.39

occurs in $LaFe_{11.7(1)}Si_{1.3(1)}$ without a change in structure. To date, all reported structural information has been based on powder X-ray diffraction data, which show just shifts in diffraction maxima across the magnetic transitions. The cubic $NaZn_{13}$-type structure adopts the centrosymmetric space group $Fm\bar{3}c$, and this has been assigned for the cubic phases $La[Fe(Fe_{12-x}Si_x)]$ ($x \leq 2.4$) for all temperatures. However, the possibility of the noncentrosymmetric space group, $F\bar{4}3c$, may not be excluded because these two space groups have identical extinction relations. Therefore, we refined our results in both space groups and results specifically for $LaFe_{11.7(1)}Si_{1.3(1)}$ and $LaFe_{10.6(1)}Si_{2.4(1)}$ are summarized in Table 1. According to the Hamilton significance test,[66] the noncentrosymmetric space group can *always* be accepted with higher than 99.5% probability below T_C, while above T_C the probability level drops to 50−97.5%, although the centrosymmetric solutions are quite acceptable. Since the literature points out that statistical distribution tests, if based only on the stronger intensities, may be strongly biased toward a noncentrosymmetric solution,[67] we must analyze the results carefully before accepting their validity.

The important geometrical effect of symmetry reduction from $Fm\bar{3}c \rightarrow F\bar{4}3c$ is to remove the {100} mirror planes that pass through the $[Fe(Fe_{12-x}Si_x)]$ icosahedral clusters, which can be accomplished by an a_u normal mode at each icosahedron. This mode, which corresponds to an a_u normal mode of the icosahedron, removes the inversion center and does *not* break the equivalence of the Fe(II)/Si sites but disrupts some of the significant Fe(II)/Si−Fe(II)/Si interatomic contacts. One way to visualize this distortion is as rotation of four triangular faces of the $[Fe(Fe_{12-x}Si_x)]$ icosahedron, faces which are normal to the {111} directions and arranged tetrahedrally around the center of the cluster. This rotation creates four smaller and four larger triangular faces normal to {111} and leaves eight isosceles triangles. Figure 10 illustrates the temperature dependences of the various interatomic distances as calculated from the two different solutions. Above T_C, the majority of the distances matched each other within three standard deviations of each other despite the difference in the atomic coordinates. However, near the Curie points, there are significant divergences (exceeding three standard deviations) for some of the Fe(II)/Si−Fe(II)/Si contacts between the noncentrosymmetric and centrosymmetric solutions. Therefore, we propose that cubic $La[Fe(Fe_{12-x}Si_x)]$ do show a slight

(65) Pecharsky, V. K.; Gschneidner, K. A., Jr. *Adv. Mater.* **2001**, *3*, 683.
(66) Hamilton, W. C. *Acta Crystallogr.* **1965**, *18*, 502.
(67) Marsh, R. E. *Acta Crystallogr.* **1981**, *B37*, 1985.
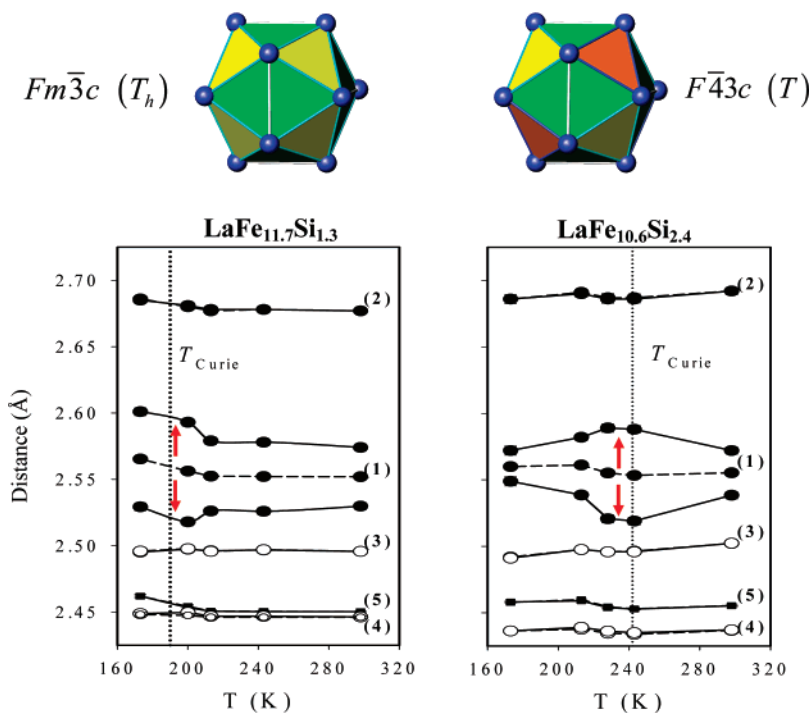
Figure 10. Temperature dependence of interatomic distances for LaFe$_{11.7(1)}$Si$_{1.3(1)}$ and LaFe$_{10.6(1)}$Si$_{2.4(1)}$ as obtained from single-crystal X-ray diffraction experiments. The same labeling scheme as in Figure 4 applies. Results from refinements in both centrosymmetric ($Fm\bar{3}c$; dashed) and noncentrosymmetric ($F\bar{4}3c$; solid) space groups are presented—only contacts (**a**) show distinct splitting. The site symmetry of the Fe(I)-centered icosahedra lowers from T_h to T (see top).

structural distortion at the magnetic transition that cannot be accurately assessed by X-ray powder diffraction alone.

Is it reasonable to accept the noncentrosymmetric solution? One method of "analysis" is to evaluate the distribution of [Fe(Fe$_{12-n}$Si$_n$)] polyhedra for a given La[Fe(Fe$_{12-x}$Si$_x$)]. In both space groups, this distribution is identical. For random distributions of Fe and Si among the Fe(II)/Si sites, the concentrations of [Fe(Fe$_{12-n}$Si$_n$)] polyhedra are given by the binomial distribution, $(12/n)x^n(1 - x)^{12-n}$. In the cubic phases, $1.3(1) \leq x \leq 2.6(1)$, the clusters [Fe(Fe$_{12}$)], [Fe(Fe$_{11}$Si)], [Fe(Fe$_{10}Si_2$)], and [Fe(Fe$_9Si_3$)] constitute more than 97% of all clusters in these structures. A glance at Figure 6, which includes the point symmetries of each [Fe(Fe$_{12-n}$Si$_n$)] configuration, reveals that *most of these clusters lack an inversion center*. Thus, although the X-ray diffraction experiment provides a "coarse-grained" average over ca. 10^6 unit cells, a noncentrosymmetric space group is not an unreasonable outcome, especially at low temperatures where atomic vibrational amplitudes are lower than at high temperatures.

To further "analyze" this transition, the total energies of a hypothetical "LaFe$_{13}$" using the refined structural parameters of LaFe$_{11.7(1)}$Si$_{1.3(1)}$ in the space groups, $Fm\bar{3}c$ and $F\bar{4}3c$, at 298 and 173 K were calculated by TB-LMTO-ASA electronic structure calculations within the LSDA. In both the cases, the noncentrosymmetric structure is energetically preferred, but the energy difference for the 298 K structures is less than 1 K/formula unit, whereas for the 173 K structure, this difference is ca. 170 K/formula unit. Therefore, the more pronounced structural distortion below the Curie point is reflected in a larger total energy difference.

In summary, refinement of the single-crystal data for the cubic NaZn$_{13}$-type phases for all temperatures below and above their corresponding Curie temperatures cannot discount a noncentrosymmetric structure. The refined atomic coordinates show largest displacements from centrosymmetry near the Curie temperatures for products with lower Si contents, i.e., those phases exhibiting greatest MCE. Therefore, the simultaneous change in the volume and magnetic structure, as well as the possible activation of the a_u normal mode around the Curie temperature through increased atomic oscillations, should all contribute to the giant MCE in the Fe-rich LaFe$_{13-x}$Si$_x$ system. The symmetry reduction that creates different sets of interatomic distances will contribute $R(\ln 2)$ to the magnetic entropy change as well as additional vibrational entropy from the shifting of the atoms. The decreasing MCE with increasing Si concentration might be due to the reductions in the volume change near T_C, as well as the decreasing changes in magnetic moments.

Electronic Structure of LaFe$_{13-x}$Si$_x$. To understand the influence of Si on the structural and magnetic properties of La[Fe(Fe$_{12-x}$Si$_x$)], TB-LMTO-ASA calculations have been performed on model structures of these compounds, focusing on "LaFe$_{13}$", "LaFe$_{11}$Si$_2$", and LaFe$_9$Si$_4$. Since "LaFe$_{13}$" is a hypothetical compound, its lattice parameter is extrapolated from the trend in lattice parameter vs Si composition. For LaFe$_{11}$Si$_2$ and LaFe$_9$Si$_4$, the experimentally determined lattice parameters and atomic coordinates are used. On the basis of the results from EHT calculations for the distribution of Si atoms in the [Fe(Fe$_{10}$Si$_2$)] icosahedron, a model for LaFe$_{11}$Si$_2$ has been constructed with an orthorhombic unit cell, space group *Cmca*, using an ordered arrangement of
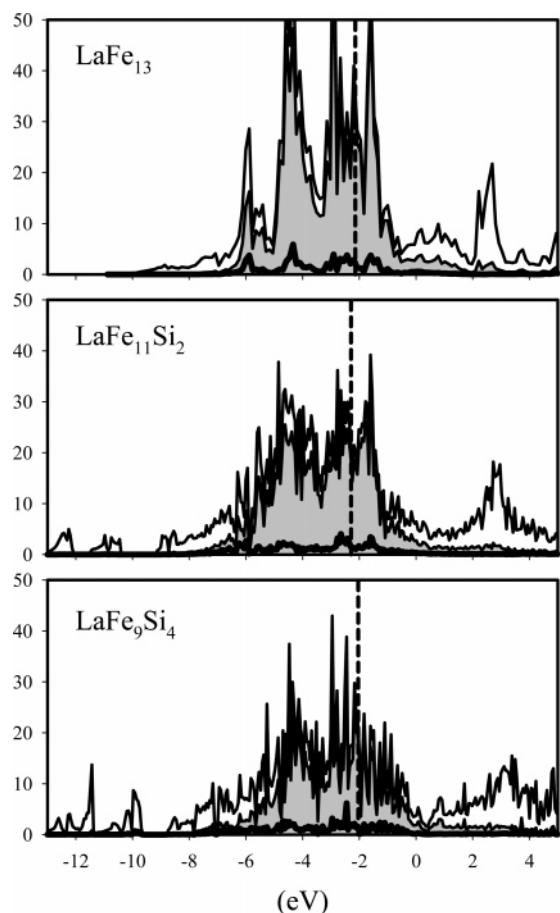
Figure 11. Total DOS curves and projections of Fe(I) (thick solid line) and Fe(II) (gray shaded region) states for "LaFe$_{13}$", "LaFe$_{11}$Si$_2$", and LaFe$_9$-Si$_4$ as calculated by TB-LMTO-ASA within the LDA. Dashed lines correspond to the respective Fermi levels.

Fe and Si atoms. We have already shown (see Figure 5) the influence of Si distributions on the tetragonal distortion of LaFe$_9$Si$_4$.

LDA Calculations. Figure 11 illustrates the total DOS curves and different partial DOS curves within the LDA for "LaFe$_{13}$", "LaFe$_{11}$Si$_2$", and LaFe$_9$Si$_4$. The overall shapes of these DOS curves are similar to one another, but there are also subtle differences. The most pronounced common features are two broad peaks near the Fermi level, which originate largely from the Fe 3d and Si 3p orbitals, as well as the position of the Fermi levels at ca. 1−1.5 eV above the minimum between these peaks (falling in the midst of the higher energy 3d−3p peak). The tails of the DOS curves below ca. −6.5 eV arises primarily from Fe 4s, 4p and Si 3s, 3p wavefunctions. Between ca. −6.5 and 0 eV (ca. 2 eV above E_F), the main contributions to the DOS are from Fe 3d orbitals. The features at ca. 2−3 eV correspond to La 4f and 5d orbitals.

The origin of the two broad peaks near the Fermi level can be explained from the orbitals associated with the transition metal icosahedra:[68,69] using a local coordinate

system at each vertex, the Fe 3d orbitals separate into 12 radial z^2 orbitals and 48 tangential xz, yz, xy, and x^2-y^2 orbitals. The tangential orbitals form 24 bonding and 24 antibonding orbitals, while the radial orbitals form four bonding, five nonbonding, and three antibonding orbitals. Through hybridization with the valence 4s and 4p, the overall pattern becomes complex, but the two peaks are dominated by the tangential orbitals of the icosahedra.

As the Si concentration increases, peaks emerge at ca. −13 to −10 eV from the Si 3s wavefunctions. Between −9 and −7 eV, contributions from Si 3p increase with Si content; in the DOS curve for "LaFe$_{13}$", these levels are primarily Fe 4s, 4p. A further effect of the Si atoms is evident above the Fermi level: the La 4f and 5d orbitals (ca. 2−3 eV) show distinctive broadening, which can be attributed to greater La−Si orbital mixing than La−Fe mixing. Near the Fermi level, however, the bandwidths of the Fe 3d orbitals for "LaFe$_{13}$", "LaFe$_{11}$Si$_2$", and LaFe$_9$Si$_4$ remain relatively constant with Si content, while the DOS values decrease monotonically. The decreasing unit cell volumes and increasing Si content lead to this result: shorter Fe−Fe distances will tend to increase the 3d bandwidth, but fewer Fe atoms in the local coordination sphere of each Fe atom will decrease this bandwidth. Regardless of the model, however, the DOS values at the Fermi level always exceed 20 states/eV/formula unit (see Supporting Information, Table S5 for selected computational results). Consequently, according to the Stoner criteria,[70] these high DOS values at the Fermi level in the LDA picture indicate probable instability to ferromagnetic behavior.

LSDA Calculations. Many different initial magnetically ordered models were explored for "LaFe$_{13}$", "LaFe$_{11}$Si$_2$", and LaFe$_9$Si$_4$ with local moments restricted to La and Fe sites. Selected results for the converged, lowest energy magnetic structure are listed in Table 2. In all cases, there was preference for a nonzero total magnetic moment; in agreement with experiment, the calculated magnetic moment per Fe atom decreases with increasing Si content. Furthermore, the converged local moments at La and Si sites are much smaller than those at the Fe sites, all of which decrease with increasing Si content, too. In all cases, the moment at the La sites opposes the moments at the Fe(II) sites; the Si moment also opposes the Fe(II) moments. An important distinction, however, exists. For "LaFe$_{13}$" and "LaFe$_{11}$Si$_2$", the Fe(I)−Fe(II) coupling is ferromagnetic (parallel), whereas it is antiferromagnetic (opposed) in LaFe$_9$Si$_4$. In fact, the local moment at the Fe(I) site in LaFe$_9$Si$_4$ converges to a much smaller value (-0.278 μ_B) than the other Fe sites ($+0.824$ and $+1.400$ μ_B); the Fe(I) moments decrease most rapidly upon increasing Si concentration. These results arise from two effects related to the increasing Si content in La-[Fe(Fe$_{12-x}$Si$_x$)]: (i) the decreasing volume creates decreasing Fe(I)−Fe(II)/Si distances and (ii) increasing Si content creates more Si neighbors to all Fe atoms. The first feature tends to favor "nonmagnetic" (i.e., degenerate "spin-up" and "spin-down" bands) solutions for the electronic structure. The

(68) Gourdon, O.; Miller, G. J. *J. Solid State Chem.* **2003**, *173*, 137.
(69) Gourdon, O.; Bud'ko, S. L.; Williams, D.; Miller, G. J. *Inorg. Chem.* **2004**, *43*, 3210.

(70) Stoner, E. C. *Proc. R. Soc. London* **1938**, *165*, 372.

Table 2. Various Results from TB-LMTO-ASA LDA and LSDA Calculations for "LaFe$_{13}$", "LaFe$_{11}$Si$_2$", and LaFe$_9$Si$_4$[a]

	"LaFe$_{13}$"		"LaFe$_{11}$Si$_2$"		LaFe$_9$Si$_4$	
	LDA	LSDA	LDA	LSDA	LDA	LSDA
E_{TOT} (eV/f.u.)	0	−0.989	0	−0.715	0	−0.267
E_F (eV)	−2.782	−2.610	−2.425	−2.268	−2.063	−2.025
$N(E_F)$ (eV^{-1})	386.85 (27.63)	105.79 (7.56)	354.20 (25.30)	178.726 (12.77)	291.92 (20.85)	214.65 (15.33)
			Magnetic Moments (μ_B)			
La		−0.508		−0.391		−0.242
Fe(I)		2.022		1.682		−0.278
Fe(II)		2.278		1.588−2.111		0.824−1.400
Si		−		−0.136		−0.087
total		28.851		20.920		8.025
total/Fe		2.219		1.902		0.892

[a] E_{TOT} = total energy relative to LDA result in eV/formula unit (f.u.); E_F = Fermi energy; $N(E_F)$ = DOS value at E_F (value in parentheses is per atom).
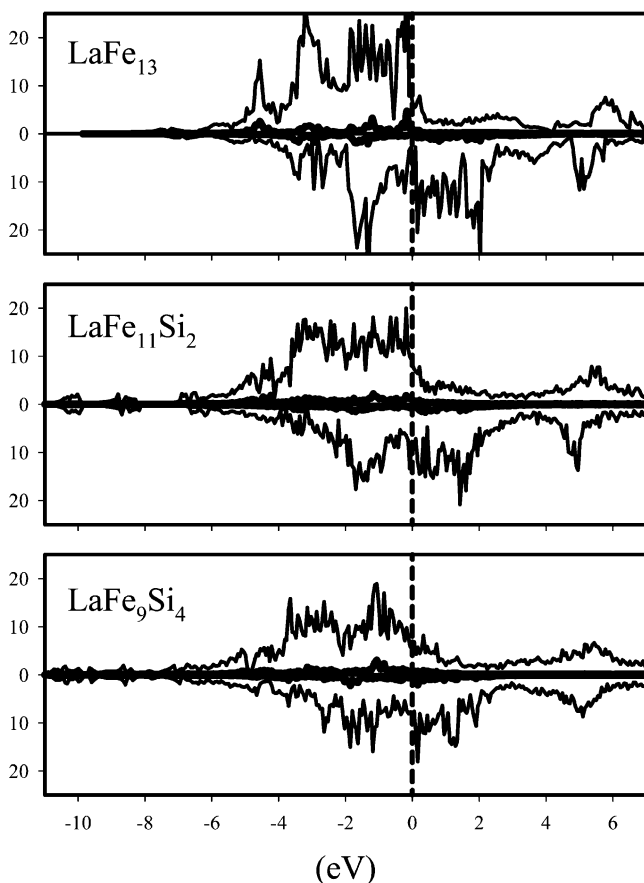
Figure 12. Total DOS for "LaFe$_{13}$", "LaFe$_{11}$Si$_2$", and LaFe$_9$Si$_4$ as calculated by TB-LMTO-ASA within the LSDA. Majority spin states are plotted upward; minority spin states are plotted downward for each case. Dashed lines correspond to the respective Fermi levels.

second item leads to lower local moments at the Fe sites with more Si neighbors via stronger Fe−Si d−p orbital overlap than Fe−Fe d−d overlap, which is a *nephelauxetic effect*.[44]

Figure 12 illustrates the majority ("spin-up") and minority ("spin-down") spin bands for "LaFe$_{13}$", "LaFe$_{11}$Si$_2$", and LaFe$_9$Si$_4$. In "LaFe$_{13}$" and "LaFe$_{11}$Si$_2$", the DOS curves show an almost-filled majority-spin band and approximately half-filled minority-spin band. As the Si content increases, the energetic splitting between the majority and minority spin bands decreases and the low-energy tails of the Fe 3d−Si 3p bands extend to lower energies (below ca. −5 eV). Again,

the increased orbital overlap in Fe−Si pairs over Fe−Fe pairs causes these effects in the DOS curves, as well as contributing to lower Fe atom exchange splittings and local magnetic moments. For LaFe$_9$Si$_4$, the distinction between majority and minority spin bands is lower than in "LaFe$_{13}$" or "LaFe$_{11}$-Si$_2$" but remains noticeable and the majority spin Fe 3d band is incompletely filled.

Although more experimental and theoretical analysis is warranted to thoroughly understand the magnetic properties of La[Fe(Fe$_{12−x}$Si$_x$)], these preliminary results indicate that the Fe-rich cases ($x \leq 2.4$) consist of "high-spin" [Fe(Fe$_{12−x}$Si$_x$)] icosahedra that are ferromagnetically coupled (the energy difference between ferromagnetically coupled and antiferromagnetically coupled clusters in "LaFe$_{13}$" is ca. 0.42 eV/formula unit). Furthermore, the Si atoms maximize their separations throughout the structure to minimize their mutual repulsive interactions. The low Si content keeps the cubic structure, and few Si neighbors surrounding each Fe atom (ca. 1−3 Si atoms at each Fe site). For the Si-rich cases, i.e., LaFe$_9$Si$_4$, the greater Si content and the distorted icosahedra create much lower local moments at the Fe(I) sites aligned antiferromagnetically to the Fe(II) moments. Nevertheless, these "intermediate-spin" clusters couple ferromagnetically. Further increasing the Si content will effectively quench the local magnetic moments at the Fe sites, as in, e.g., β-FeSi$_2$.[59]

Relationship between Si Concentration and Curie Temperature. The magnetic behavior of La[Fe(Fe$_{12−x}$Si$_x$)] is complex: while the unit cell volumes and saturation magnetizations decrease with increasing x, the corresponding Curie temperatures increase.[9,25] For itinerant magnets, the saturation magnetization is related to the difference in "spin-up" and "spin-down" electrons, which can be calculated within the LSDA. Curie temperatures, on the other hand, provide a measure of the effective exchange interactions, which have been estimated via mean-field approaches.[71] In rare-earth−iron intermetallic compounds specifically, the Curie temperature is strongly affected by the strength of the Fe−Fe exchange coupling, which sensitively depends on the Fe−Fe interatomic distance.[72] According to Givord et al., the distance at which the Fe−Fe exchange interaction

(71) Kikuchi, R. *Phys. Rev.* **1951**, *81*, 988. Vaks, V. G.; Samolyuk, G. D. *Sov. Phys. JETP* **1999**, *88*, 89. Xu, J. L.; van Schilfgaarde, M.; Samolyuk, G. D. *Phys. Rev. Lett.* **2005**, *94*, 097201.

Table 3. Comparison of Fe−Fe Distances and Magnetic Ordering Temperatures in Various Fe-Containing Intermetallics

compound	structure type	Fe−Fe distance (Å)	T_C (K)	ref
α-Fe	W	2.48	1044	28
LaFe$_{10.9}$Al$_{2.1}$	NaZn$_{13}$	2.47	200	29
LaFe$_{11.4}$Al$_{1.6}$	NaZn$_{13}$	2.46	204	30
Lu$_2$Fe$_{17}$	Th$_2$Ni$_{17}$	2.39	771	31
Ce$_2$Fe$_{17}$	Ce$_2$Fe$_{17}$	2.38	235	32
Nd$_2$Fe$_{14}$B	Nd$_2$Fe$_{14}$B	2.40	585	24

switches between ferromagnetic and antiferromagnetic is ca. 2.45 Å: antiferromagnetic for shorter distances and ferromagnetic for longer contacts.[57] Either an increase in Fe−Fe interatomic distances or a decrease in the fraction of short Fe−Fe bonds are expected to enhance the overall Fe−Fe exchange couplings and, consequently, the Curie temperature. Previous investigations have tried to explain the change in Curie temperature for NaZn$_{13}$-type intermetallic compounds by analyzing the Fe−Fe interactions, which is sensitive to the Fe−Fe distance and the number of nearest neighbors,[10,11,13,14] but the underlying physical mechanism is not well understood to date.

On the basis of our own investigation of Fe−Fe bond distances using single-crystal refinements of several La[Fe(Fe$_{12-x}$Si$_x$)] compounds, there are two kinds of bond length variations: (1) inter-icosahedral distances shorter than 2.45 Å decrease with Si content and (2) intra- and inter-icosahedral contacts exceeding 2.45 Å show little change with Si content (some even expand). Similar Fe−Fe bond distances also exist in several ferromagnetic and antiferromagnetic materials, listed in Table 3. Although the shortest Fe−Fe distances are similar among several different materials, we see a range of magnetic interactions. Therefore, relatively short Fe−Fe distances do not necessarily imply antiferromagnetic ordering between nearest Fe−Fe interactions. Extensive investigations of volume effects in several interstitial[73] and substitutional modifications[74] of R$_2$Fe$_{17}$ and RFe$_{12-x}$M$_x$ compounds have also shown that antiferromagnetic interactions are not simply related to short interatomic Fe−Fe distances. However, analysis of interatomic distances shows that the fraction of contacts shorter than 2.45 Å decreases upon increasing Si content, which reduces the effect of antiferromagnetic Fe−Fe exchange interactions and leads to an increase in the Curie temperature.

There are more appropriate theories, such as the spin fluctuation theory of Mohn and Wohlfarth, to describe the Curie temperature enhancement in terms of changes in the electronic structure.[75] Mohn and Wohlfarth explained the large increases of Curie temperature for substitutional modifications of Re$_2$Fe$_{17}$ by a decrease in spin fluctuations, which is caused by lowering the DOS at the Fermi level upon substitution. To explain the increase of T_C in LaFe$_{13-x}$Si$_x$ qualitatively, we can also use the following relation obtained

for iron-rich alloys in the spin-fluctuation theory of Mohn and Wohlfarth,[76]

$$T_C = \frac{M_0^2}{10\mu_B^2\chi_0} \tag{1}$$

where M_0 is the magnetic moment at 0 K and χ_0 is the exchange-enhanced susceptibility, given by[76]

$$\frac{1}{\chi_0} = \frac{1}{4\mu_B^2}\left(\frac{1}{N_\uparrow(E_F)} + \frac{1}{N_\downarrow(E_F)} - 2I\right) \tag{2}$$

where $N_\uparrow(E_F)$ and $N_\downarrow(E_F)$, respectively, are the integrated majority- and minority-spin DOS values at the Fermi energy and I is a measure of the strength of the exchange interaction in the metal. For LaFe$_{13-x}$Si$_x$, the values of M_0 drop with increasing x, so that χ_0 becomes the determining factor for the Curie temperature variation in this series. Since the parameter I remains rather constant regardless of the local environment of Fe in its alloys,[77] the quantitative behavior of χ_0 in eq 2 is determined mainly by the quantities $N_\uparrow(E_F)$ and $N_\downarrow(E_F)$. According to the results of our LSDA calculations for "LaFe$_{13}$", "LaFe$_{11}$Si$_2$", and LaFe$_9$Si$_4$ (see Table 2), the total DOS at the Fermi level decreases upon Si concentration. Therefore, this can lead to an increasing Curie temperature.

Summary

A thorough structural and preliminary theoretical investigation of La[Fe(Fe$_{12-x}$Si$_x$)] to study their structure−bonding−property relationships is reported. The main results of this work include (1) La[Fe(Fe$_{12-x}$Si$_x$)] crystallize in the cubic NaZn$_{13}$-type structure for the range 1.3(1) ≤ x ≤ 2.6-(1), and the tetragonal Ce$_2$Ni$_{17}$Si$_9$-type structure for 3.2(1) ≤ x ≤ 5.0(1). In the range 2.6 ≤ x ≤ 3.2, a two-phase mixture occurs. (2) Bond analyses at various temperatures indicate that the noncentrosymmetric space group $F\bar{4}3c$ provides a viable atomic arrangement over the centrosymmetric space group $Fm\bar{3}c$, especially at temperatures near and below the corresponding Curie temperatures for the cubic phases. The relationship between these two space groups is an "a_u" normal mode associated with the icosahedral clusters. Thus, the giant MCE observed for cubic LaFe$_{13-x}$Si$_x$ examples can result from coupling between magnetic ordering and a structural transformation beyond just the magnetovolume effect. (3) Si atoms maximize their mutual separations, which contributes to both enthalpic and entropic influences on the observed crystal symmetries and atomic distributions. (4) The calculated magnetic moments at the Fe sites decrease with increasing Si concentration due to more effective Fe 3d−Si 3p orbital overlap. (5) The increasing Curie temperatures with increasing Si content can be understood using the spin-fluctuation theory of Mohn and Wohlfarth through changes in the DOS values at the Fermi level.

(72) Marasinghe, G. K.; Exekwenna, C.; James, W. J.; Hu, Z.; Yelon, W. B. *J Appl. Phys.* **1997**, *81*, 5103.
(73) Jaswal, S. S.; Grandjean, F.; Long, G. J.; Buschow, K. H. J., Eds. Proc. NATO-ASI, Series E281, *Interstitial Intermetallic Alloys*; Kluwer Academic Publishers: Dordrecht, 1995; p 411.
(74) Woods, J. P.; Patterson, B. M.; Fernando, A. S.; Jaswal, S. S.; Welipitya, D.; Sellmyer, D. J. *Phys. Rev.* **1995**, *B51*, 1064.
(75) Mohn, P.; Wohlfarth, E. P. *J. Phys. F: Metal Phys.* **1987**, *17*, 2421.
(76) Wohlfarth, E. P. *Phys Lett.* **1962**, *3*, 17.
(77) Janak, J. F. *Phys. Rev.* **1977**, *B16* (1), 255.

Supporting Information Available: The results of phase analysis and refinement, tables of crystallographic data, and related information for crystals **1**−**7, 9**; structural data at various temperatures (173, 213, 228, 243, 293 K) for $LaFe_{11.7(1)}Si_{1.3(1)}$, $LaFe_{11.1(1)}$-$Si_{1.9(1)}$, and $LaFe_{10.6(1)}Si_{2.4(1)}$; and TB-LMTO-ASA relative total energies of various magnetic models of "$LaFe_{13}$" and $LaFe_9Si_4$. This material is available free of charge via the Internet at http://pubs.acs.org.

IC701311B